Properties and Performance of the Orbital-Angular-Momentum Modes in Wireless Communication

Chen Feng and Jinhong Li(✉)

School of Electronics and Information,
Northwestern Polytechnical University, Xi'an, China
lijinhong@mail.nwpu.edu.cn

Abstract. The orbital-angular-momentum (OAM) mode multiplexing is one of the promising ways to improve the efficiency of the spectrum utilization of the network in the Internet of Things (IoT). In this article, the propagation properties and the communication performance of the OAM modes in radio frequency are studied. The transverse patterns for the single mode, two/three superimposed modes are discussed, while the influences of the mode number and the propagation distance on the beam width are analyzed. Based on 2FSK and 2PSK modulations the bit error rate (BER) of OAM modes are found varying with both the mode and the receiving radius of the array antennas. By analyzing the BER, it is found that when both the transmitting antenna and the transmitting power are fixed, also the noise power is the same, an OAM mode can have different optimal receiving radii in the single mode transmission and in the mode multiplexing transmission. These results will be helpful in optimizing the OAM mode receiving system and may have applications in the network of the IoT.

Keywords: Orbital angular momentum · IoT · Vortex

1 Introduction

Nowadays, we are standing on the brink of a new ubiquitous computing and communication era [1,2]. The development and application of the IoT are based on numerous micro-sensor networks, and the collected data by numerous sensors are transmitted through wireless communication [3]. As we all know, the number of wireless communication devices are growing fast, so it has led to the congestion on the available bands [4,5]. Therefore, its vital to find new methods to solve this problem.

Supported by the Seed Foundation of Innovation and Creation for Graduate Students in Northwestern Polytechnical University.

B. Li et al. (Eds.): IoTaaS 2019, LNICST 316, pp. 514–526, 2020.
https://doi.org/10.1007/978-3-030-44751-9_43

Electromagnetic (EM) vortex technology, as a new wireless communication technology, utilizes the orbital angular momentum (OAM) characteristics to transmit information efficiently. The waves with OAM has been studied a lot in optical frequency [6–10], and also is proposed to increase the spectral efficiency in optical wireless communication systems [5,11,12]. It was recently shown that the OAM can be used in the radio frequency (RF) and is not restricted to the optical frequency range [13]. In 1992, Allen et al. discovered that a helically phased light beam with the OAM property can be obtained when Laguerre-Gaussian (LG) modes were generated from Hermite-Gaussian (HG) modes through using cylindrical lenses [14,15]. By using the same principle, in 2012, Tamburini et al. [4] used a helical parabolic antenna to generate OAM modes in radio beams, and realized OAM multiplexing transmission at the radio frequency. Theoretically, an EM wave can carry an infinite number of OAM modes at the same frequency where each mode is orthogonal to each other [16]. Thus the multiplexing based on OAM modes can greatly increase the efficiency spectrum utilization in free space. Also because of the orthogonality of different OAM modes the EM waves with OAM modes have a good anti-jamming ability. Therefore the application of OAM in wireless communication is going to become a trend in EM wave studies. However, the performance of the EM beams with OAM in wireless communication channels is not quite clear.

In the paper, the theoretical background of OAM modes is introduced firstly, then the formula for generating EM wave carrying OAM modes with circular array antenna is given. The propagation properties of the EM waves with OAM modes and their performance in a wireless communication system will be analyzed in detail in Sect. 3.

2 Theory

It is well known that EM radiation can carry both linear momentum and angular momentum [6,17]. The total angular momentum is composed of spin angular momentum (SAM) and OAM, which can be described in the following expression:

$$\mathbf{J} = \epsilon_0 \int \mathbf{r} \times \mathrm{Re}\left[\mathbf{E} \times \mathbf{B}^*\right] \mathrm{d}V. \tag{1}$$

Where $\mathbf{E}$ and $\mathbf{B}$ are the electric and magnetic vector fields, $\mathbf{r}$ is the position vector, and ϵ_0 is the vacuum permittivity, respectively. The angular momentum can be decomposed into a polarization dependent intrinsic rotation (i.e. SAM) and an extrinsic rotation (i.e. OAM) [18]. Then the total angular momentum $\mathbf{J}$ can be given by the sum [19]

$$\mathbf{J} = \mathbf{L} + \mathbf{S}, \tag{2}$$

where $\mathbf{L}$ represents the OAM of the electromagnetic radiation, and the mode number is denoted by l, while $\mathbf{S}$ is the SAM whose mode number is s with $s = \pm 1$.

An EM beam with OAM is also called an EM vortex beam, and its expression can be written as

$$\mathrm{E}(\mathrm{r}, \varphi, \omega) = \mathrm{A}(\mathrm{r}, \varphi) \exp(\mathrm{i}l\varphi) \exp(\mathrm{i}\omega t), \tag{3}$$

Where $\mathrm{A}(\mathrm{r}, \varphi)$ is the amplitude of this vortex wave, r represents the radial distance, φ is the azimuth angle, and ω is the frequency of the EM wave. Here as we introduced before, l is the mode of OAM which represents how many 2π of the phase change as the φ goes from 0 to 2π in the transverse plane of the wave. It can be concluded from the formula that OAM can carry infinite topological charges theoretically. Thus unlike linear momentum, it can provide a new degree of freedom for the beams in wireless communication systems. In addition, different OAM modes are orthogonal to each other and they can be multiplexed/demultiplexed together, thus the channel capacity will be increased.

There are many ways to generate vortex waves, such as using a helicoidal parabolic antenna [4], adopting the spiral phase plate [20] and applying a uniform circular array (UCA) [19,21]. Among these methods, maybe the most common way is using a UCA in which each element is fed by the same signal, but with a successive phase element to element, such that after a full turn, the phase of the composed wave has been incremented by an integer multiple l of 2π (see Fig. 1). The N elements of this antenna array are located equidistantly around the perimeter of the circle and are phased with phase difference between each element $\Delta\phi = 2\pi l/N$. According to [13], for an array of N antenna elements, the largest OAM number l_{max} should satisfy $|l_{max}| < N/2$.

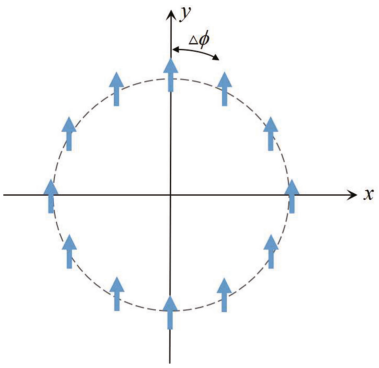

Fig. 1. Structure of the antenna array configuration.

The electric field in the far field of such an array antenna can be calculated by using the radiation theory of the array antennas, and for any detection point $P(r, \theta, \varphi)$ in this field (see Fig. 2) can be expressed as [19]:

$$\begin{aligned}\boldsymbol{E}(r,\theta,\varphi) &= -\boldsymbol{j}\frac{\mu_0\omega}{4\pi}\sum_{n=0}^{N-1} e^{\mathrm{i}l\varphi_n}\int \frac{e^{\mathrm{i}k|r-r'_n|}}{|\boldsymbol{r}-\boldsymbol{r}'_n|}dV'_n \\ &\approx -\boldsymbol{j}\frac{\mu_0\omega d}{4\pi}\cdot\frac{e^{\mathrm{i}kr}}{r}\sum_{n=0}^{N-1} e^{-\mathrm{i}(k\cdot r_n - l\varphi_n)} \\ &\approx -\boldsymbol{j}\frac{\mu_0\omega d}{4\pi}\frac{e^{\mathrm{i}kr}}{r}N\mathrm{i}^{-l}e^{\mathrm{i}l\varphi}J_l(kR\sin\theta),\end{aligned} \tag{4}$$

where $\boldsymbol{j}$ is the constant current density vector of the dipole, d is the electric dipole length, μ_0 is the magnetic conductivity in the vacuum, ω and k are the circular frequency and wave vector, respectively. $J_l(kR\sin\theta)$ is the Bessel function of the first kind, $\varphi_n = 2\pi n/N$ $(n = 0, 1, 2, \cdots, N-1)$ is the azimuthal angle of the array element position, and R is the radius of the array. Also in Eq. (4) the frequency dependence is suppressed for brevity, and from here on we will not discuss that dependence.

As an example, the intensity distribution of the radiation field from this array antennas is shown in Fig. 3, where the total number of the elements is 15, the topological charge or the OAM mode is chosen as 2 and the propagation distance is 1 m. It is clear to see that there is a dark hole (i.e. the intensity minimum) in the beam center that is the reason for another name of the beam with OAM – 'doughnut beam'.

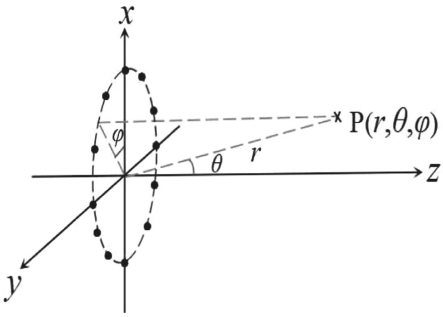

Fig. 2. Diagram of uniform circular antenna array.

3 Simulation and Discussion

In this part, the propagation properties of EM waves with OAM mode and their performance in communication systems will be analyzed. In this article the UCA is adopted to generate and receive OAM waves. The number of the antenna elements in both the transmitting and receiving ends always is set to be 15 (i.e., $l_{max} \leq 7$), and the frequency is set as $f = 3\,\mathrm{GHz}$, i.e., $\lambda = 0.1\,\mathrm{m}$. Here the transmit array radius is denoted by R_t and in this part R_t is chosen as λ. The receive array radius is denoted by R_r, and from here on we use n and p to represent the nth and the pth element of the transmitter and receiver, respectively.

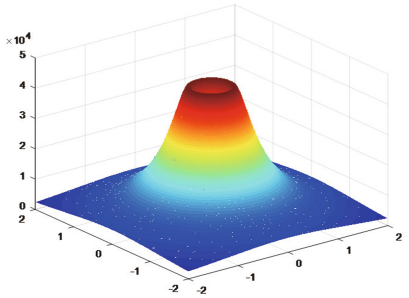

Fig. 3. Intensity distribution of EM wave with OAM mode. Here $N = 15$, $l = 2$ and $z = 1\,\mathrm{m}$.

3.1 Propagation Properties

The phase distribution in the transverse plane with $z = 10\lambda$ (propagation distance) is shown in Fig. 4 for different OAM modes, i.e. $l = 0, 1, 2$. The change in color from red to blue corresponds to a change in phase of 2π. Here $l = 0$ indicates there is no OAM, and it is clear to see that the phase does not rotate along the azimuthal angle, which means that the wave with $l = 0$ is a plane EM wave. When $l = 1$, the phase of radiation electric field changes 2π during one revolution, while $l = 2$, the phase changes 4π. The result shows that the EM wave with OAM mode has a helical phase front, and the phase variation is l times 2π.

Let us examine the propagation properties of the EM wave with one mode, and here the mode 3 is chosen. Except the propagation distance which is a variable in this part, the other parameters are the same with them in Fig. 4. The intensity distribution of electric field in the transverse plane with different propagation distances is shown in Fig. 5, where the color from blue to red corresponds to the 0 and maximum value of the intensity. From here on, in each plot of intensity, the intensity maximum is normalized to 1. We can see in Fig. 5 that there always exists a dark core in the intensity pattern, which means that the vortex or the phase singularity is located at the beam center. From this figure one can get that as the wave propagates, the beam spreads wider and wider.

Now we will look at the influence of the topological charge, i.e. OAM mode on the beam propagation. In Fig. 6 the intensity distribution of the electric field with different OAM modes are shown, where the propagation distance is $z = 10\lambda$. It can be seen that when the mode is getting bigger, the radius of the intensity pattern becomes wider and the hollow in the beam center is wider too. In another word, the bigger of l is, the stronger the wave diverges.

Therefore, we can conclude that increasing the OAM mode and/or the propagation distance, the width of the beam will be larger, which is very important in the receiving end of the wireless communication system.

When the OAM multiplexing is applied, the superposition of multi-OAM modes will occur, and since the helical phase distribution of the EM waves

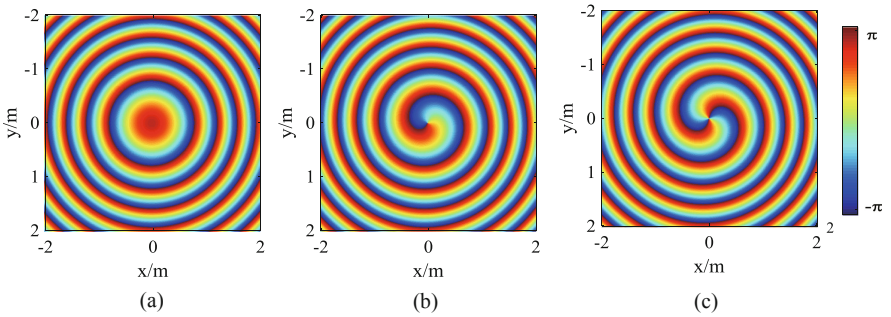

Fig. 4. Phase distribution of the OAM. (a) $l = 0$ (b) $l = 1$ (c) $l = 2$.

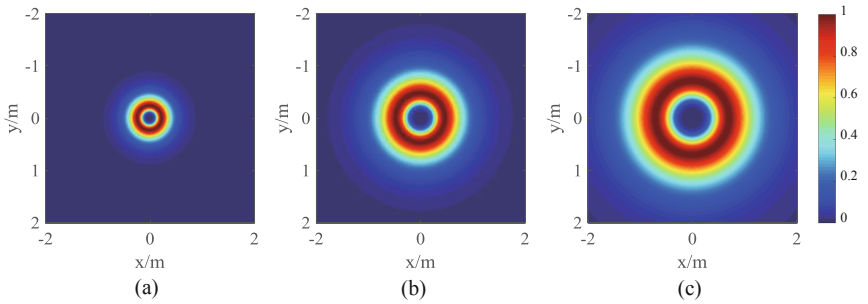

Fig. 5. Intensity distribution at the transverse planes with different propagation distances in the case of $l = 3$. (a) $z = 3\lambda$ (b) $z = 6\lambda$ (c) $z = 9\lambda$.

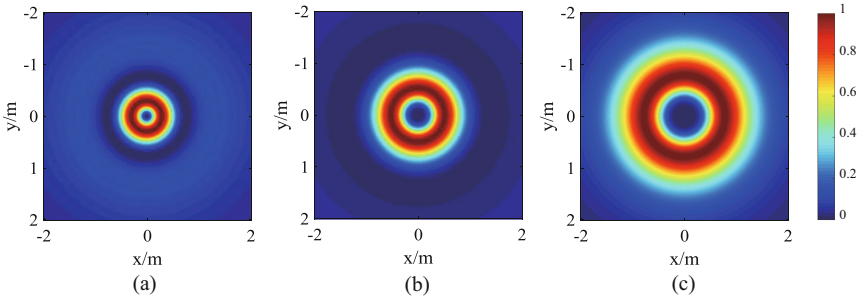

Fig. 6. Intensity distribution at the transverse planes for the different topological charges. (a) $l = 1$ (b) $l = 2$ (c) $l = 3$. Here $z = 10\lambda$

with OAM modes, the superposition patterns of different modes are usually not uniformally distributed and as we will see that they will show quite interesting patterns. First, the superposition patterns of two different modes are shown in Fig. 7 ($z = 3\lambda$) and Fig. 8 ($z = 10\lambda$). Plot (a) in these two figures is the superposition of the waves with mode 1 and 2, plot (b) is for mode 1 and 3,

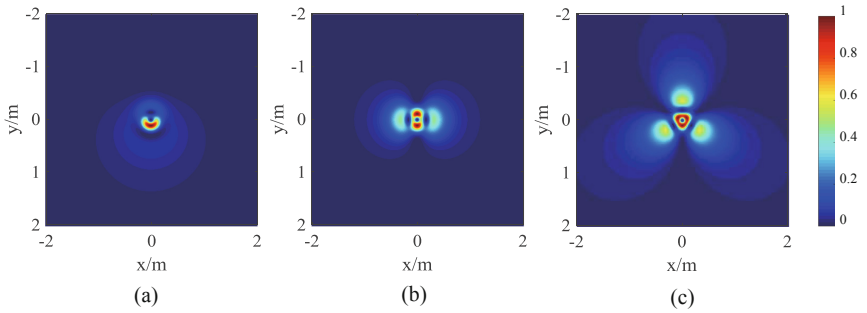

Fig. 7. Intensity distribution of the superposition of two different OAM modes. (a) $l = 1, 2$, (b) $l = 1, 3$, (c) $l = 1, 4$. Here $z = 3\lambda$.

and plot (c) is for mode 1 and 4. One can observe that the number of the bright spots (i.e. the dark red regions) is 1 in plot (a), is 2 in plot (b) and is 3 in plot (c). These results indicate that the number of bright spots is equal to $N = |l_1 - l_2|$, which is coincident with that in [22]. Note in these figures the radii of the transmitting array antennas for the waves with any OAM mode are all chosen as $R_t = \lambda = 0.1$ m. We also want to state that if R_t is selected differently for each mode, the number of the bright spots are easier to be observed. By comparing Fig. 7 with Fig. 8, one also can see the diffusion effect of the EM waves with two OAM modes.

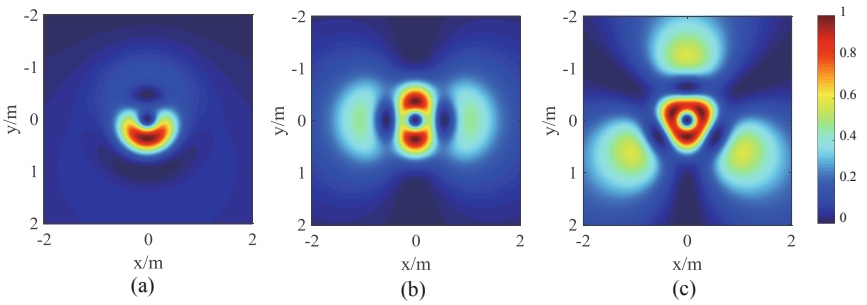

Fig. 8. Intensity distribution of the superposition of two different OAM modes. (a) $l = 1, 2$, (b) $l = 1, 3$, (c) $l = 1, 4$. Here $z = 10\lambda$.

When the number of the superimposed OAM modes is more 2, the superposition pattern will become more complicated which is not easy to describe the number of the bright spots in a simple equation. For instance when three OAM modes are superimposed, there can be 1, 2 and 3 bright spots, which is not easy to connect with their mode number difference. This is shown in Figs. 9 and 10, where the propagation distance is 3λ and 10λ respectively. Comparing

the intensity distributions of single mode, two superimposed modes and three superimposed modes, it is not hard to find that at the same propagation distance the intensity maxima with more modes are closer to the beam center. This result also indicates that if a good efficiency wants to be obtained in the receiving end, the position of the receiving antenna should be adjusted with the number of the modes involved in the EM wave.

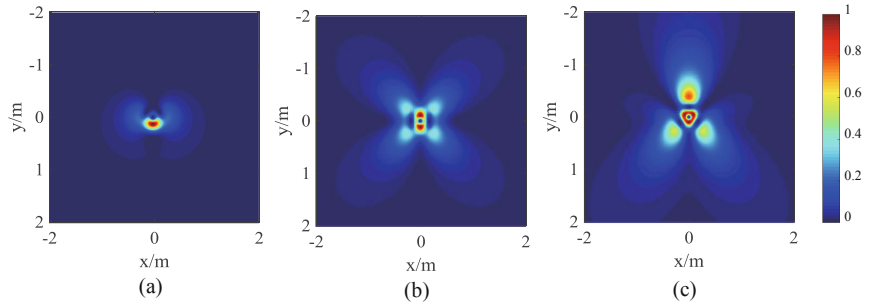

Fig. 9. Intensity distribution of the superposition of three different OAM modes. (a) $l = 1, 2$, (b) $l = 1, 3$, (c) $l = 1, 4$. Here $z = 3\lambda$. (a) $l = 1, 2, 3$, (b) $l = 1, 3, 5$, (c) $l = 1, 4, 6$. Here $z = 3\lambda$.

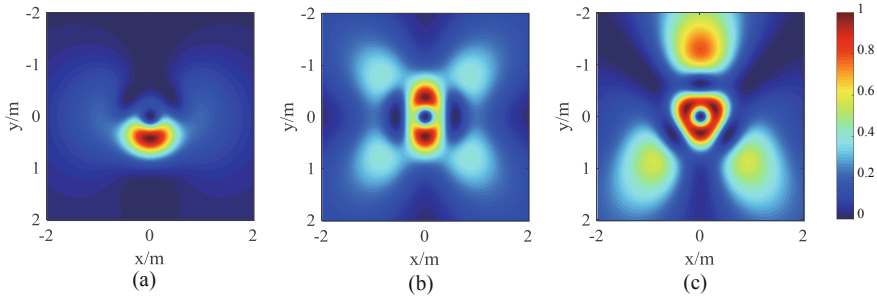

Fig. 10. Intensity distribution of the superposition of three different OAM modes. (a) $l = 1, 2, 3$, (b) $l = 1, 3, 5$, (c) $l = 1, 4, 6$. Here $z = 10\lambda$.

3.2 Performance of OAM Modes in Communication System

In the previous section, the propagation properties of the EM waves with OAM modes are discussed, here we focus our attention on the performance of the OAM modes in communication systems and the bit error rate (BER) is adopt to measure this performance.

EM waves with OAM not only diffuse during propagation, but also have a certain amount of attenuation [23]. Therefore, OAM-link budget should be considered in the OAM communication system. For the transmitting and receiving antennas are both UCA, the OAM-link budget estimation between two facing arrays can be expressed as [24]:

$$\frac{P_r}{P_t}(l) = \left|\frac{b_l^{OAM}}{a_l^{OAM}}\right|^2 = \left|\sum_{p=0}^{N-1}\sum_{n=0}^{N-1}\frac{\beta}{N}e^{-\mathrm{i}l\theta_{np}}e^{-\mathrm{i}kr_{np}}\frac{\lambda}{4\pi r_{np}}\right|^2, \tag{5}$$

where P_r and P_t are receiving power and transmitting power, respectively. $r_{np} = \sqrt{z^2 + R_t^2 + R_r^2 - 2R_tR_r\cos\theta_{np}}$, $\theta_{np} = 2\pi(\frac{n-p}{N})$, β contains all the variables associated with the antenna system configuration.

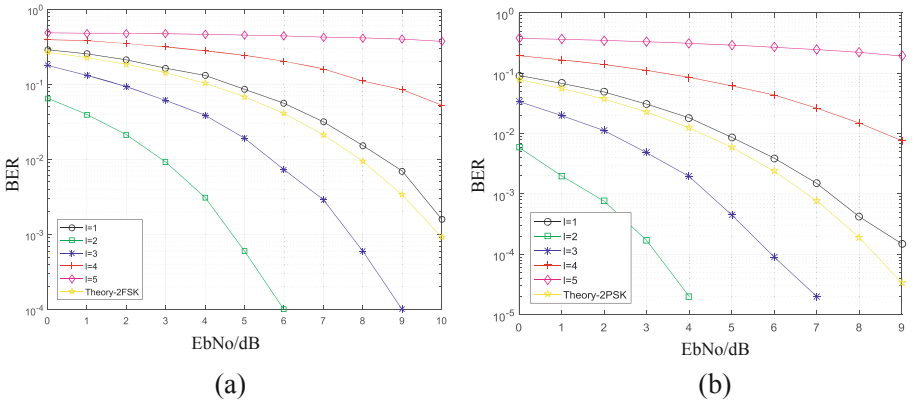

Fig. 11. The BER of different l under the same noise power. Here $N = 15$, $R_t = \lambda$, $R_r = 6\lambda$, $z = 10\lambda$. (a) Based on 2FSK, (b) Based on 2PSK.

According to Eq. (5) and the theory discussed in previous two sections, the curves of BER for different modes l under the same noise power are illustrated in Fig. 11, where plot (a) and plot (b) are based on 2FSK and 2PSK modulation respectively. Here the transmit array radius is also set as $R_t = \lambda = 0.1$ m, and the receive array radius $R_r = 6\lambda = 0.6$ m. First, one can see that two different modulations 2FSK and 2PSK do not influence the BER strongly. Second, it can be observed that the BER for each l is different with each other, and it follows this rule: $\mathrm{BER}(l = 2) < \mathrm{BER}(l = 3) < \mathrm{BER}(l = 1) < \mathrm{BER}(l = 4) < \mathrm{BER}(l = 5)$. Also the BER for $l = 2$ and $l = 3$ is lower than the theoretical value. This can be explained as the different attenuation for each l. The different attenuation will lead to different power received at the same receiving position for different modes, which has a straight effect on the BER. The small BER for $l = 2$ and $l = 3$ is obtained because at the receiving radius $R_r = 6\lambda$ the power received for these two modes are bigger than others. This also indicates that if both the

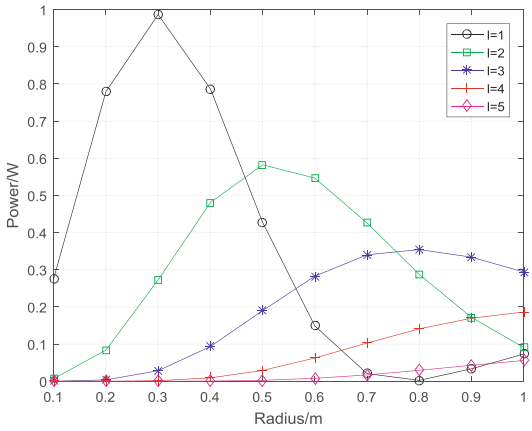

Fig. 12. The receiving power of selected l with different receiving radius. Here $N = 15$, $R_t = \lambda$, $z = 10\lambda$.

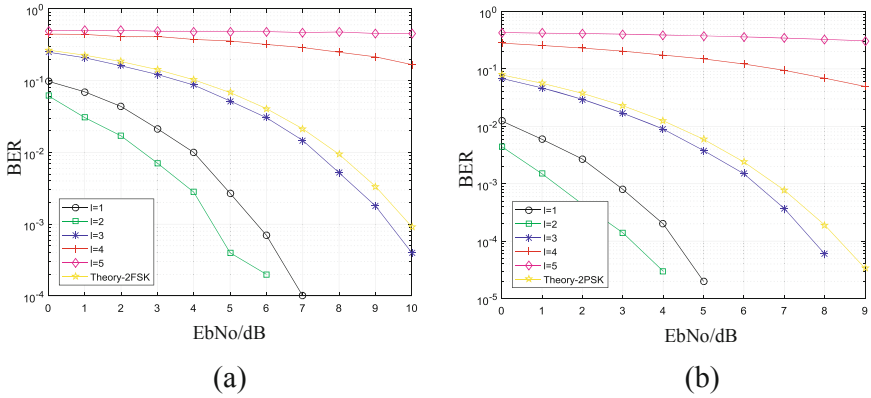

Fig. 13. The BER of different l under the same noise power. Here $N = 15$, $R_t = \lambda$, $R_r = 5\lambda$, $z = 10\lambda$. (a) Based on 2FSK, (b) Based on 2PSK.

transmitting antenna and the transmitting power are fixed and the noise in the channel also does not change, for each mode l, there exists an optimal receiving radius.

In Fig. 12 the receiving power for different l at varying receiving radius are shown. Here the transmitting power is set as $P_t = 1$ W. It is clear to see that at different receiving radius the power for different modes may follow different orders. For example when $R_r = 6\lambda = 0.6$ m, the power PW received for different modes satisfy: $PW(l = 2) > PW(l = 3) > PW(l = 1) > PW(l = 4) > PW(l = 5)$. Since the noise power is the same and the BER is inversely proportional to the receiving power, the BER in the Fig. 11 follows the rule of $\text{BER}(l = 2) < \text{BER}(l = 3) < \text{BER}(l = 1) < \text{BER}(l = 4) < \text{BER}(l = 5)$. As a test, in Fig. 13,

when the receiving radius $R_r = 5\lambda = 0.5$ m, the BER of different l under the same noise power are simulated and shown. It can be seen that the BER follows: $\mathrm{BER}(l=2) < \mathrm{BER}(l=1) < \mathrm{BER}(l=3) < \mathrm{BER}(l=4) < \mathrm{BER}(l=5)$, which is consistent with the order of the power received at $R_r = 5\lambda = 0.5$ m in Fig. 12.

As discussed above, for any OAM mode it has its own optimal receiving radius. Here, applying the same method used in Fig. 12 the optimal receiving radius for different modes can be calculated and given in the first two columns of Table 1. It can be seen that the optimal receiving radius will get bigger as the OAM mode l increases. This is also consistent with our conclusion in previous section that the larger the mode l is, the stronger the diffusion of the EM wave gets. In addition, by repeating the same steps we also obtain the optimal receiving radius for the EM wave with two superimposed modes, as is shown in the last two columns of Table 1. From this table, one also can find that generally the optical receiving radius for the superimposed two modes is smaller than that for a single mode, which also can be illustrated in the propagation patterns in previous sections (see Figs. 5, 6, 7 and 8). This result indicates that the communication performance of an OAM mode in the OAM mode multiplexing is different from that in the single mode transmission.

Table 1. The optimal receiving radius of different modes.

Single mode	R_r/m	Superimposed modes	R_r/m
$l=1$	0.29	$l_1=1,\ l_2=2$	0.38
$l=2$	0.52	$l_1=1,\ l_2=3$	0.37
$l=3$	0.78	$l_1=1,\ l_2=4$	0.32
$l=4$	1.12	$l_1=2,\ l_2=4$	0.61
$l=5$	1.50	$l_1=2,\ l_2=5$	0.57
$l=6$	1.88	$l_1=2,\ l_2=6$	0.53

4 Conclusions

In this article the UCA is used for both the transmitting and receiving the EM waves with OAM modes, and the propagation properties and the communication performance of the OAM modes are studied. First, it is found that the increasing the OAM mode and/or the propagation distance will enlarge the width of the beam with OAM. Second, when the number of the superimposed OAM modes is more 2, the superposition pattern will become more complicated and its bright spots number can not be described by the mode number difference. Third, two different modulations 2FSK and 2PSK do not have strong effect on the BER of OAM modes, but the mode l does. For each mode, it has its own attenuation during the mode propagation, which leads to the difference BER for different modes. At last, the optimal receiving radii for the OAM modes are proposed and

calculated for both the different single modes and the different superimposed modes. Our result shows that the communication performance of an OAM mode relies on whether it is in the mode multiplexing or not, and also depends on how many modes are used in the multiplexing. We believe that our findings will be quite useful in improving the receiving techniques for OAM modes, and can be applied to the IoT. For example, smart home connects all kinds of devices through the IoT technology to realize the full-ranged information interaction and Intelligent Transportation System also integrates different installations to ensuretrafficsafety. The large amount of data generated during these devices makes it difficult to transfer data efficiently. The orthogonality between different modes of OAM can deal with this problem and improve information interaction capability.

References

1. Peña-López, I., et al.: ITU internet report 2005: the internet of things (2005)
2. Lin, J., Yu, W., Zhang, N., Yang, X., Zhang, H., Zhao, W.: A survey on internet of things: architecture, enabling technologies, security and privacy, and applications. IEEE Internet Things J. **4**(5), 1125–1142 (2017)
3. Ashton, K.: That internet of things. RFID J. **22**(7), 97–114 (2009)
4. Tamburini, F., Mari, E., Sponselli, A., Thidé, B., Bianchini, A., Romanato, F.: Encoding many channels on the same frequency through radio vorticity: first experimental test. New J. Phys. **14**(3), 033001 (2012)
5. Chen, C., Wang, W., Wu, J., et al.: Visible light communications for the implementation of internet-of-things. Opt. Eng. **55**(6), 060501 (2016)
6. Allen, L., Barnett, S.M., Padgett, M.J.: Optical Angular Momentum. IoP Publishing, Bristol (2003)
7. Pang, X.: Gouy phase and phase singularities of tightly focused, circularly polarized vortex beams. Opt. Commun. **338**, 534–539 (2015)
8. Zhao, X., Zhang, J., Pang, X., Wan, G.: Properties of a strongly focused gaussian beam with an off-axis vortex. Opt. Commun. **389**, 275–282 (2017)
9. Pang, X., Miao, W.: Spinning spin density vectors along the propagation direction. Opt. Lett. **43**(19), 4831–4834 (2018)
10. Li, J., Zhang, J., Li, J.: Optical twists and transverse focal shift in a strongly focused, circularly polarized vortex field. Opt. Commun. **439**, 284–289 (2019)
11. Wang, J., et al.: Terabit free-space data transmission employing orbital angular momentum multiplexing. Nat. Photon. **6**(7), 488 (2012)
12. Li, M.: Orbital-angular-momentum multiplexing optical wireless communications with adaptive modes adjustment in internet of things networks. IEEE Internet Things J. **6**, 6134–6139 (2019)
13. Thidé, B., et al.: Utilization of photon orbital angular momentum in the low-frequency radio domain. Phys. Rev. Lett. **99**(8), 087701 (2007)
14. Allen, L., Beijersbergen, M.W., Spreeuw, R., Woerdman, J.: Orbital angular momentum of light and the transformation of laguerre-gaussian laser modes. Phys. Rev. A **45**(11), 8185 (1992)
15. Demeter, Á., Kertész, C.Z.: Simulation of free-space communication using the orbital angular momentum of radio waves. In: 2014 International Conference on Optimization of Electrical and Electronic Equipment (OPTIM), pp. 846–851. IEEE (2014)

16. Molina-Terriza, G., Torres, J.P., Torner, L.: Management of the angular momentum of light: preparation of photons in multidimensional vector states of angular momentum. Phys. Rev. Lett. **88**(1), 013601 (2001)
17. Loudon, R., Baxter, C.: Contributions of john henry poynting to the understanding of radiation pressure. Proc. R. Soc. Lond. A **468**(2143), 1825–1838 (2012)
18. Barnett, S.M.: Optical angular-momentum flux. J. Opt. B: Quantum Semiclass. Opt. **4**(2), S7 (2001)
19. Mohammadi, S.M., et al.: Orbital angular momentum in radio-a system study. IEEE Trans. Antennas Propag. **58**(2), 565–572 (2009)
20. Tamburini, F., Mari, E., Bo, T., Barbieri, C., Romanato, F.: Experimental verification of photon angular momentum and vorticity with radio techniques. Appl. Phys. Lett. **99**(20), 321 (2011)
21. Gong, Y., et al.: Generation and transmission of OAM-carrying vortex beams using circular antenna array. IEEE Trans. Antennas Propag. **65**(6), 2940–2949 (2017)
22. Ke, X., Pu, X.: Generation of orbital angular momentum superpositions and its test. Infrared Laser Eng. **47**(4), 56–61 (2018)
23. Cagliero, A., De Vita, A., Gaffoglio, R., Sacco, B.: A new approach to the link budget concept for an oam communication link. IEEE Antennas Wireless Propag. Lett. **15**, 568–571 (2015)
24. Nguyen, D.K., Pascal, O., Sokoloff, J., Chabory, A., Palacin, B., Capet, N.: Antenna gain and link budget for waves carrying orbital angular momentum. Radio Sci. **50**(11), 1165–1175 (2015)